A&A manuscript no.
(will be inserted by hand later)

Your thesaurus codes are:
12 (02.01.2; 02.02.1; 02.13.2; 08.13.2; 09.10.1; 11.10.1)

ASTRONOMY
AND
ASTROPHYSICS

Magnetically driven superluminal motion from rotating black holes

Solution of the magnetic wind equation in Kerr metric

Christian Fendt and Jochen Greiner

Astrophysikalisches Institut Potsdam, An der Sternwarte 16, D-14482 Potsdam, Germany

Received ?? ; accepted ??

Abstract. We have investigated magnetically driven superluminal jets originating from rotating black holes. The stationary, general relativistic, magnetohydrodynamic wind equation along collimating magnetic flux surfaces has been solved numerically. Our jet solutions are calculated on a global scale over a spatial range from several to several 1000 gravitational radii. Different magnetic field geometries were investigated, parameterized by the shape of the magnetic flux surface and the magnetic flux distribution. For a given magnetic flux surface we obtain the complete set of physical parameters for the jet flow. In particular, we apply our results to the Galactic superluminal sources GRS 1915+105 and GRO 1655-40.

Our results show that the observed speed of more than 0.9 c can be achieved in general by magnetohydrodynamic acceleration. The velocity distribution along the magnetic field has a saturating profile. The asymptotic jet velocity depends either on the plasma magnetization (for a fixed field structure) or on the magnetic flux distribution (for fixed magnetization). The distance where the asymptotic velocity is reached is below the observational resolution for GRS 1915+105 by several orders of magnitude. Further, we find that highly relativistic speeds can be reached also for jets *not* emerging from a region close to the black hole, if the flow magnetization is sufficiently large.

Motivated by the huge size indicated for the Galactic superluminal knots of about 10^9 Schwarzschild radii, we point out the possibility that the jet collimation process in these sources may be less efficient and therefore intrinsically different to the AGN. The plasma temperature rapidly decreases from about 10^{10}K at the foot point of the jet to about 10^6K at a distance of 5000 gravitational radii from the source. Temperature and the mass density follow a power law distribution with the radius. The jet magnetic field is dominated by the toroidal component, whereas the velocity field is dominated by the poloidal component.

Key words: Accretion, accretion disks Black hole physics – MHD – Stars: mass loss – ISM: jets and outflows – Galaxies: jets

Send offprint requests to: Christian Fendt, e-mail: cfendt@aip.de

1. Introduction

1.1. Relativistic jets and Galactic superluminal motion

Apparent superluminal jet motion originating in the close environment of a rotating black hole is observationally indicated for two classes of sources concerning mass and energy output. One class is the family of radio loud active galactic nuclei (hereafter AGN). In the AGN standard model highly relativistic jet motion is explained by *magnetohydrodynamic* processes in a black hole - accretion disk environment (for a review see Blandford 1990). Jets are magnetically accelerated and possibly also collimated by magnetic forces. However, the detailed interaction process of the magnetized black hole - accretion disk system which is believed to lead to the ejection of high velocity blobs is not yet fully understood.

The other class are galactic binary systems for which radio observations have also detected superluminal motion (see reviews of Fender 2000 or Greiner 2000). The two most prominent examples are the high energy sources GRS 1915+105 (Mirabel & Rodriguez 1994) and GRO 1655-40 (Hjellming & Rupen 1995; Tingay et al. 1995). The deprojected jet speed of both sources is $\gtrsim 0.9\,c$ and surprisingly similar, although for GRS 1915+105 also a higher velocity component has been observed recently (Fender et al. 1999). GRO 1655-40 is a binary consisting of a $7.02 \pm 0.22\,\mathrm{M}_\odot$ black hole and a $2.3\,\mathrm{M}_\odot$ F-subgiant (Orosz & Bailyn 1997) at a distance of 3 kpc. GRS 1915+105 is at 10–12 kpc distance (Fender et al. 1999), but the component masses of the presumed binary are not known. Order of magnitude estimates based on X-ray variability and QPO properties range from 10–80 $\mathrm{M}_\odot$ (Morgan et al. 1997, Greiner et al. 1998). As for the AGN jet sources, observational evidence for a black hole - accretion disk system is found also for the Galactic superluminal sources. Observations have also indicated that accretion disk instabilities may be related to jet ejection (Greiner et al. 1996, Belloni et al. 1997, Mirabel et al. 1998). Therefore, the jet formation process for extragalactic jets and their Galactic counterparts may be the same, although the mechanism that accelerates and collimates the GRS 1915+105 ejecta is yet unclear (Rodriguez & Mirabel 1999).

Optical polarization measurements have been obtained for the microquasar GRO J1655-40 (Scaltriti et al. 1997, Gliozzi et al. 1998). The polarization angle is approximately parallel to the accretion disk plane. The amount of polarization has been found to vary smoothly with the orbital phase, being smallest at binary phase 0.7–0.8. It has been noted that the occasionally observed X-ray dips occur at the same phase interval (Ueda et al. 1998, Kuulkers et al. 1998) suggesting that it may be related to either a thickening of the disk rim at the impact site of the accretion stream from the companion or the overflow of this stream above/below the disk. The orbital polarization modulation rules out a synchrotron origin in the jet, and implies the presence of electron scattering plasma above the accretion disk which is asymmetrically distributed or asymmetrically illuminated. The existence of such scattering plasma is consistent with the interpretation of the iron features as observed with ASCA as absorption lines and edges in a thick, cool torus of column $N_{\rm H} > 10^{23}{\rm cm}^{-2}$ (Ueda et al. 1998).

The relativistic speed observed for the Galactic superluminal sources ($\sim 0.9 - 0.98\,c$ de-projected) corresponds to a bulk Lorentz factor of $\gamma = 2 - 5$ although this number is not very accurate (e.g. Fender et al. 1999). Therefore, for any theoretical investigation of these objects at least special relativity has to be taken into account. If the superluminal motion originates close to a black hole, also general relativistic effects may become important.

The ejection of matter itself is not a stationary process. In GRS 1915+105 also repeated emission of knots is observed (Rodriguez & Mirabel 1999). X-ray and radio observations suggest that a wide range of ejected mass and ejection frequency is possible.

Though the galactic jet sources are nearby, they are not better resolved spatially because the distance ratio between AGN and microquasars is smaller than their mass ratios. Nevertheless, an important implication may also come from the observed size of the superluminal knots which are observationally resolved. In the case of GRS 1915+105 the characteristic dimension of the 'jet' is 35 mas, equivalent to 7×10^{15} cm at a distance of 12.5 kpc (Rodriguez & Mirabel 1999). We emphasize that such a knot size corresponds to $\sim 10^9$ Schwarzschild radii for $R_{\rm S} = 1.5 \times 10^6\,(M/5\,{\rm M}_{\odot}){\rm cm}$! This is a huge factor and may be in distinctive difference to the AGN jets. Similarly, the VLBA data show the core as a collimated jet down to a distance of 10 AU from the central source with an opening angle of $< 10^{\circ}$ (see Mirabel & Rodriguez 1999) corresponding to $10^7\,(M/5{\rm M}_{\odot})$ Schwarzschild radii. The length of the radio jet is about 100 AU.

However, when interpreting the observed emission region, one has to keep in mind that this region may not represent the jet flow itself, but some *part* of another, larger, structure. For example, in some extragalactic jet sources there is indication that the knots travel along helical trajectories, believed to be prescribed by a large-scale helical magnetic field of an almost cylindrically collimated jet (Zensus et al. 1995; Camenzind & Krockenberger 1992).

In GRO 1655-40 the motion of the radio knots is complicated and requires (at least) precession between different ejections (Hjellming & Rupen 1995). The knot structures in GRS 1915+105 remained fixed implying that the whole knot moves with the same speed without spatial diffusion and with an axial velocity profile more or less constant.

Based on minimum energy arguments and only relativistic electrons responsible for the synchrotron radiation in the knots of GRS 1915+105 , Rodriguez & Mirabel (1999) derive a magnetic field strength of about 50 mG to 7 mG, the decrease resulting from the expansion of the knot. They also estimate the rest mass of a knot of $\geq 10^{23}$ g, and together with (steady) photon luminosity of $\simeq 3 \times 10^{38}\,{\rm erg\,s}^{-1}$, exclude radiation as driving mechanism for the knots.

1.2. Theory of magnetic jets

From the introductory remarks it is clear that a quantitative analysis of superluminal motion must take into account both magnetohydrodynamics (hereafter MHD) and (general) relativity.

The first theoretical formulation of the electromagnetic force-equilibrium in Kerr space-time around rotating black holes was given by Blandford & Znajek (1977) and Znajek (1977), who discovered the possibility of extracting rotational energy and angular momentum from the black hole electromagnetically.

Camenzind (1986, 1987) formulated a fully relativistic stationary description of MHD flows, basically applicable to any field geometry. The structure of such collimating jet magnetospheres in the case of Kerr space time was presented by Fendt (1997). Solutions of the so-called wind equation in Kerr geometry (see below) considering the stationary plasma motion along the magnetic field were discussed by Takahashi et al. (1990), however, applied for an accretion flow and not for a wind flow.

While the asymptotic structure of the propagating jets becomes more and more understood with the help of time-dependent magnetohydrodynamical, also relativistic, simulations (e.g. Nishikawa et al. 1997; Mioduszewski et al. 1997; Hardee et al. 1998), the process of jet formation itself and the collimation of the outflow region is a task still too complex for numerical simulations. The involved length scales and gradients require a high resolution in grid size and time stepping. Koide et al. (1998, 2000) were first to perform general relativistic MHD simulations of jet formation close to the black hole. In their model, the interaction of an initially cylindrical magnetic field with an Keplerian accretion disk results first in an inflow of matter towards the black hole. This accretion stream interacts with the hydrostatic corona around the black hole giving rise to a relativistic gas pressure driven jet. At larger radii a magnetically driven wind is initiated from the accretion disk. The simulations were performed for less than two rotations of the inner disk (corresponding to less than 0.02 rotations of the disk at the outer edge of the grid). Although these results of the first fully general relativistic MHD simulations look indeed very exciting, some objections can be raised about the underlying model. The initial condition applied is that of a hydrostatic corona around a black hole, an assumption which is not compatible with the boundary of a black hole horizon. Such a configuration is not stable and will immediately collapse. Since the simulation lasts only over a few Keplerian periods, the ejection of the jet components could might be only a relict of the unstable initial condition and might not be present over the long-term evolution.

1.3. *Aim of the present study*

In this paper, a stationary magnetic jet flow along a given magnetic flux surface is investigated in the context of general relativity. Due to the stationary approach, we cannot treat any time-dependent phenomena. Our emphasis is to trace the *large scale* behavior of the flow from it's origin close to the black hole to large distances. This is an essential point in particular for the Galactic superluminal sources because of the possible huge spatial extension of the jets compared to the central black hole. The stationary model allows for a *global* treatment of the jet flow, i.e. an investigation over a large range of magnitudes for density and magnetic field strength. This is not yet feasible with time-dependent MHD codes presently available. In particular, we address the following topics.

- For a given geometry of the magnetic field, which are the resulting jet *dynamical parameters* as velocity, density or temperature?
- How important are the effects of general relativity? Does the superluminal flow indeed originate very close to a black hole?
- From the investigation of different field geometries we expect some hints to the jet opening angle and the length scale of the collimation process.

The structure of this paper is as follows. In Sect. 2, basic equations for relativistic magnetospheres are reviewed in the context of Kerr metrics. In Sect. 3, the model underlying our numerical calculations is discussed. We present our numerical results in Sect. 4 and discuss solutions with different geometry and jet parameters. We summarize our paper in Sect. 5.

2. Description of a MHD flow in Kerr metric

Under the assumptions of axisymmetry, stationarity and infinite conductivity, the MHD equations reduce to a set of two basic equations describing the local force-balance across the field and along the field (for references, see, e.g., Blandford & Znajek 1977; Thorne et al. 1986; Camenzind 1986, 1987; Okamoto 1992; Beskin & Pariev 1993, Beskin 1997).

The trans-field or *Grad-Shafranov equation* determines the field structure, whereas the *wind equation* describes the flow dynamics along the field. Due to the stationarity assumption, certain conservation laws apply. The total energy density, the total angular momentum density, the mass flow rate per flux surface and the iso-rotation parameter are conserved quantities along the surfaces of constant magnetic flux (Camenzind 1986).

In this paper the motion of a magnetized plasma is calculated from the wind equation. The plasma moves along a prescribed axisymmetric magnetic flux surface which originates in a region close to a rotating black hole.

2.1. *Space-time around rotating black holes*

The space-time around a rotating black hole with a mass M and angular momentum per unit mass a is described using Boyer-Lindquist coordinates with the line element

$$ds^2 = \alpha^2 dt^2 - \tilde{\omega}^2 \, (d\phi - \omega dt)^2 - (\rho^2/\Delta) \, dr^2 - \rho^2 \, d\theta^2 , \quad (1)$$

where t denotes the global time, ϕ the angle around the axis of symmetry, r, θ similar to there flat space counterpart spherical coordinates, and where geometrical units $c = G = 1$ have been applied (see Appendix A for further definitions). The horizon of the Kerr black hole is located at $r_{\rm H} = M + \sqrt{M^2 - a^2}$. We will normalize all radii to gravitational radii $r_{\rm g} = r_{\rm H}(a = M) = M$. The angular velocity of an observer moving with zero angular momentum (ZAMO) is $\omega = (d\phi/dt)_{\rm ZAMO}$, corresponding to the angular velocity of the differentially rotating space. The lapse function is $\alpha = (d\tau/dt)_{\rm ZAMO}$ describing the lapse of the proper time τ in the ZAMO system to the global time t.

2.2. *Description of the electromagnetic field*

In the 3+1 split of Kerr space time (Thorne et al. 1986) the electromagnetic field $\boldsymbol{B}, \boldsymbol{E}$, the current density $\boldsymbol{j}$, and the electric charge density $\rho_{\rm c}$ can be described very similar to the usual expressions, if measured by the ZAMO's according to the locally flat Minkowski space. These local experiments then have to be put together by a global observer for a certain global time using the lapse and shift function for the transformation from the local to the global frame.

With the assumption of axisymmetry a magnetic flux function can be defined measuring the magnetic flux through a loop of the Killing vector $\boldsymbol{m} = \tilde{\omega}^2 \nabla \phi$,

$$\Psi(r,\theta) = \frac{1}{2\pi} \int \boldsymbol{B}_{\rm p} \cdot d\boldsymbol{A} \, , \qquad \boldsymbol{B}_{\rm p} = \frac{1}{\tilde{\omega}^2} \nabla \Psi \wedge \boldsymbol{m}, \quad (2)$$

corresponding to the magnetic flux through an area $\pi (r \, \sin\theta)^2$ around the symmetry axis (in the limit of Minkowski space).

With the assumption of a degenerated magnetosphere, $|B^2 - E^2| >> |\boldsymbol{E} \cdot \boldsymbol{B}| \simeq 0$ an 'angular velocity of field lines' can be derived from the derivative of the time component of the vector potential $\Omega_{\rm F} = \Omega_{\rm F}(\Psi) = -2\pi c (dA_0/d\Psi)$. We will denote this quantity with the term 'iso-rotation parameter'.

2.3. *The wind equation*

It has been shown that a stationary, polytropic, general relativistic MHD flow along an axisymmetric flux surface $\Psi(r,\theta)$ can be described by the following *wind equation* for the poloidal velocity $u_{\rm p} \equiv \gamma v_{\rm p}/c$,

$$u_{\rm p}^2 + 1 = -\sigma_{\rm m} \left(\frac{E}{\mu}\right)^2 \frac{k_0 k_2 + \sigma_{\rm m} 2 k_2 M^2 - k_4 M^4}{(k_0 + \sigma_{\rm m} M^2)^2}\,, \qquad (3)$$

where

$$k_0 \;=\; g_{33}\Omega_{\rm F}^2 + 2 g_{03}\Omega_{\rm F} + g_{00},$$
$$k_2 \;=\; 1 - \Omega_{\rm F}\frac{L}{E},$$
$$k_4 \;=\; -\left(g_{33} + 2 g_{03}\frac{L}{E} + g_{00}\frac{L^2}{E^2}\right) / \left(g_{03}^2 - g_{00} g_{33}\right)$$

(Camenzind 1986, Takahashi et al. 1990). The Alfvén Mach number M is defined as $M^2 = 4\mu n u_{\rm p}^2 / \tilde{B}_{\rm p}^2$, with the proper particle density n, the specific enthalpy μ, and a poloidal magnetic field $\tilde{B}_{\rm p} = B_{\rm p}/(g_{00)} + g_{03}\Omega_{\rm F})$, rescaled for mathematical convenience. For a polytropic gas law with the index $\Gamma \equiv n/m$, the wind equation (3) can be converted into a polynomial equation,

$$\sum_{i=0}^{2n+2m} A_i(x;\Psi,\Phi;\Omega_{\rm F};E,L,\sigma_\star)\, u_{\rm P}^{i/m} = 0\,, \qquad (4)$$

(Camenzind 1987, Englmaier 1993, Jensen 1997), where the coefficients A_i are now defined as functions of the normalized cylindrical radius $x = R/r_{\rm g}$ (see Appendix B). The shape of the axisymmetric magnetic flux surface Ψ is prescribed as function $z(x;\Psi)$. The flux function $\Phi = \sqrt{-g}\tilde{B}_{\rm p}$ describes the opening of the flux surface. The faster Φ decreases the faster magnetic energy is converted into kinetic energy. We define the dimensionless magnetization parameter [1] at the 'injection' point $x_\star$ following Takahashi et al. (1990),

$$\sigma_\star = \frac{\Phi_\star^2}{4\pi m_{\rm p} I_{\rm p\star}}, \qquad (5)$$

measuring the Poynting flux in terms of particle flux $I_{\rm p} \equiv \sqrt{-g}\, n u_{\rm p}$. The magnetization determines the maximum energy available for plasma acceleration and thus determines also the asymptotic poloidal velocity. The other wind parameters are total energy density E, total angular momentum L, and the iso-rotation parameter $\Omega_{\rm F}$.

We choose the polytropic index $\Gamma = 5/3$ for a hot relativistic proton-electron plasma (a hot electron-positron plasma would imply $\Gamma = 4/3$). Then, at each radius x the polynomial equation (4) has $2n + 2m = 16$ solutions. Some of these mathematical solutions have no physical meaning, e.g. because $u_{\rm p}^2$ is negative. The remaining physical solutions form a bunch of different curves in the $u_{\rm p}(x)$-diagram representing different solution branches (see our solution S1 in Appendix C, Fig. C1). The unique branch of the 'wind' solution starts at a small radius with small velocity continuing outwards with increasing velocity. For an other parameter choice also 'accretion' branches can be found, starting from a large radius with small velocity and continuing inwards with increasing velocity (not shown in Fig. C1).

However, not for all parameters E, L, σ there exist *physical* solutions which are continuous functions of x and therefore defined along the whole flux surface. It is well known that at the magnetosonic points the wind equation (3) becomes singular (see Camenzind 1986, Takahashi et al. 1990). Regularity of the solution requires a flow velocity equal to the speed of the MHD waves in order to obtain a smooth (self-consistent) transition at the magnetosonic points. In order to match astrophysical boundary conditions we fix the following parameters by our model,

– *the 'injection' radius*, $x_\star$, the location where the matter couples to the magnetic field. This radius also determines the iso-rotation parameter $\Omega_{\rm F}$.
– *the 'injection' velocity* $u_{\rm p\star} = u_{\rm p}(x_\star)$, defining the initial kinetic energy.
– *the Alfvén radius* $x_{\rm A}$, which fixes the total angular momentum of the flow.

The critical wind solution for a given flux surface can then be found by varying the flow parameters in Eq. (4). Due to numerical convenience, we vary

– *the sound speed* $c_{\rm s\star}$ at the injection radius, defining the initial density (or gas pressure and temperature),
– *the magnetization* parameter at the injection point $\sigma_\star(\Psi) = \Phi_\star^2/(4\pi m_{\rm p} I_{\rm p\star})$.

In turn, the condition of a regular flow at the slow magnetosonic point fixes the sound speed and, thus, jet mass flow rate.

3. The model assumptions

3.1. The model in general

Observationally the jet phenomenon of AGN, young stellar objects and microquasars is always connected to the signatures of an accretion disk. We therefore assume a similar disk-jet scenario for the jet formation in *Galactic* superluminal jet sources. In general our model geometry follows the standard model for jet formation in AGN (cf. Blandford 1990).

Two typical length scales enter the problem. (i) The gravitational radius $r_{\rm g}$ measures the influence of gravity on the metric. (ii) The asymptotic light cylinder $R_{\rm L}$ describes the influence of rotation on the electrodynamics.

3.2. The central black hole

The black hole mass and angular momentum determine the geometry of space. Since we use dimensionless equations normalized to the gravitational radius, our results scale with the mass of the black hole. For parameter estimates we assume

[1] Note that this definition for the magnetization varies from the original Michel magnetization parameter $\sigma_{\rm M} = \Phi_{\rm M}^2/4\pi f_{\rm M} c R_{\rm L}^2$, where $\Phi_{\rm M}$ is the magnetic flux, $f_{\rm M}$ the mass flux and $R_{\rm L}$ the light cylinder. This comes from the fact that the general relativistic equations have been normalized to the gravitational radius, whereas the special relativistic equations have been normalized to the light cylinder

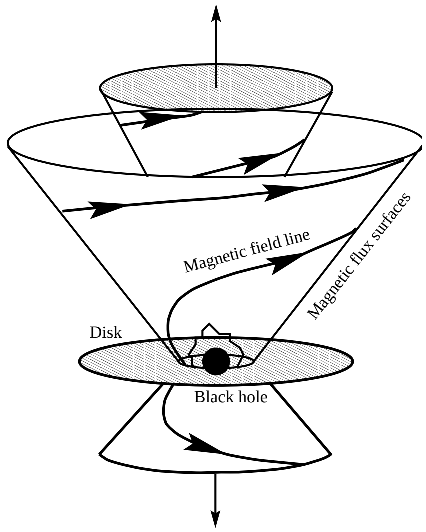

Fig. 1. Model geometry applied for our numerical calculations. The poloidal field structure is prescribed as magnetic flux surfaces with different opening angle. These flux surfaces different foot point radii along the accretion disk (not visible). The central source is a black hole implying that general relativistic effects have to be taken into account. The toroidal field follows from the solution of the wind equation.

a black hole mass of $5\,\mathrm{M}_\odot$ which is about the value inferred for the galactic superluminal sources. The angular momentum a as the other black hole parameter is not known for any of the relativistic jet sources. Interpretation of the high effective temperatures of the accretion disk as well as the stable QPO frequency (as Thirring-Lense effect) suggests that $a \gtrsim$0.9 for GRS 1915+105 and GRO 1655-40 (Zhang et al. 1997). Theoretically, one may expect a rapidly rotating black hole because of angular momentum conservation during the collapse and also accretion of angular momentum from the accretion disk (King & Kolb 2000). Here, we choose $a = 0.8$, a value which is not extreme, but clearly different to Schwarzschild metric. The rotation rate of the black hole is defined as $\Omega_{\rm H} \equiv \omega(r_{\rm H}) = a/(2Mr_{\rm H})$. The Kerr parameter a does not influence the solution of the wind equation directly. However, for rotating black holes the marginally stable orbit $r_{\rm ms}$ is closer to the horizon, $r_{\rm ms} = 6r_{\rm g}$ for $a = 0$ and $r_{\rm ms} \simeq r_{\rm g}$ for $a \simeq 1$). Thus, if the jet magnetic field is anchored just outside the marginally stable orbit, this means that for a rapidly rotating black hole also the maximum angular speed of the jet foot points increases by a factor of $6^{3/2} = 14.5$. Correspondingly, the light cylinder radius of the jet moves inward by the same factor.

In addition to the well-known special relativistic light cylinder, the differential rotation of the space ω leads to the formation of a second light surface. At this position the 'rotational velocity' of the field lines relative to the ZAMO equals the speed of light (see Blandford & Znajek 1977). The position of the two light surfaces $\tilde{\omega}_{\rm L}$ is defined by $\tilde{\omega}_{\rm L}^2 = (\pm\alpha\, c/(\Omega_{\rm F} - \omega))^2$, where the $+$ $(-)$ sign holds for the outer (inner) light surface with $\Omega_{\rm F} > \omega$ ($\Omega_{\rm F} < \omega$). However, these light surfaces have no direct implication for the MHD flow. In the limit of a strong magnetization, the MHD Alfvén surfaces (for inflow and outflow) approach the corresponding light surfaces.

3.3. The accretion disk

X-ray observations of GRS 1915+105 detected strong intensity variations indicating major instabilities of an accretion disk (Greiner et al. 1996). Belloni et al. (1997) find that the highly variable X-ray spectra could be explained if the inner disk is alternatively removed and replenished due to a thermal-viscous instability. Simultaneous X-ray and infrared observations of GRS 1915+105 revealed evidence for a disk–jet interrelation (Eikenberry et al. 1998, Mirabel et al. 1998). The observed flares in the X-ray and IR bands have a consistent offset delay of ~ 30 min indicating an origin from the same event.

The accretion rate in GRS 1915+105 and GRO J1655-40 can be determined from the observed X-ray luminosities (e.g. Greiner et al. 1998). Depending on the chosen efficiency (5% in non-rotating versus 42% in maximally rotating black holes) the accretion rate ranges between $1 - 9 \times 10^{-7}\mathrm{M}_\odot\mathrm{yr}^{-1}$ (GRS 1915+105) and $0.8 - 7 \times 10^{-8}\mathrm{M}_\odot\mathrm{yr}^{-1}$ (GRO J1655-40), respectively.

From the theoretical point of view an accretion disk surrounding the black hole is the essential component concerning magnetic jet formation. It is considered to be responsible for the following necessary ingredients for jet formation, propagation, and collimation.

- The *generation of the magnetic field*. In contrast to stellar jets the magnetic field of jets from black holes cannot be supplied by the central object but has to be generated by the surrounding accretion disk. Dynamo action in general relativistic accretion disks were discussed by Khanna & Camenzind (1996a, 1996b) and Brandenburg (1996).
- The *mass loading of the jet*. The accreting material becomes partly diverted into the jet. Evidently, no mass outflow is possible from the black hole itself, in difference to a stellar wind. Self-similar accretion-ejection mechanisms were investigated by Ferreira (1997).
- The *electric current* system. Differential rotation of the disk is also responsible for driving the poloidal electric current system in the jet magnetosphere. Such a current extracts angular momentum from the disk and eventually allows for mass accretion into the central object.

3.4. model parameters for the wind motion

3.4.1. The magnetization parameter

The leading parameter for the wind solution along a fixed poloidal field is the magnetization parameter (5). Renormalization to astrophysical units gives

$$\sigma_\star(\Psi) = \frac{\Phi_\star^2}{4\pi m_{\rm p} I_{{\rm p}\star}} \rightarrow \frac{B_{{\rm p}\star}^2 R_\star^4}{c\dot{M}_{\rm jet}(\Psi) r_{\rm g}^2} = \frac{B_{{\rm p}\star}^2 r_{\rm g}^2}{c\dot{M}_{\rm jet}(\Psi)}\left(\frac{R_\star}{r_{\rm g}}\right)^4 \quad (6)$$

where $\dot{M}_{\rm jet}(\Psi) \simeq\simeq 4\pi m_{\rm p} n_\star c u_{{\rm p}\star} R_\star^2$ is the jet mass flux enclosed by an area of radius $R_\star$. A first order estimate of the magnetization can be derived from the disk equipartition field strength. Then, with a reasonable assumption on the jet mass flow rate related to the disk accretion rate, this gives the jet magnetization. Although the equipartition field strength is model-dependent, the different models (e.g. either advection dominated disk or standard disk, either Kramer's opacity or Thomson scattering) give rather similar results. A self-similar advection dominated disk model with the accretion rate $\dot{M}_{\rm acc}$ gives

$$B_{\rm eq} \simeq 2.5\times 10^9 {\rm G}\ \alpha_{\rm vis}^{-\frac{1}{2}} \left(\frac{M}{5{\rm M}_{\odot}}\right)^{-\frac{1}{2}} \left(\frac{\dot{M}_{\rm acc}}{\dot{M}_{\rm E}}\right)^{\frac{1}{2}} \left(\frac{R}{r_{\rm g}}\right)^{-\frac{5}{4}}, \tag{7}$$

where $\dot{M}_{\rm E} = 1.1\times 10^{-7} (M/5{\rm M}_{\odot})\,{\rm M}_{\odot}{\rm yr}^{-1}$ is the Eddington luminosity and $\alpha_{\rm vis}$ is the viscosity parameter (see e.g. Narayan et al. 1998). In comparison, an optically thin standard accretion disk with Thomson opacity gives $B_{\rm eq} \simeq \sqrt{8\pi P} = \sqrt{8\pi a T^4/3} \simeq 1.8\times 10^8 {\rm G}\, \alpha_{\rm vis}^{-1/2} (M/5{\rm M}_{\odot})^{-1/2} (R/r_{\rm g})^{-3/4}$ (see Blandford 1990). Note that these estimates are only valid within certain limits of the accretion rate and the disk radius. Using the advection dominated disk model equipartition field strength, we obtain the following estimate for the magnetization at the injection radius,

$$\sigma_{\star}(\Psi) = 16 \frac{1}{\alpha_{\rm vis}} \left(\frac{M}{5{\rm M}_{\odot}}\right) \left(\frac{\dot{M}_{\rm jet}}{\dot{M}_{\rm acc}}\right)^{-1} \left(\frac{R_{\star}}{r_{\rm g}}\right)^{3/2} \tag{8}$$

A comparison with the original Michel magnetization parameter must take into account a factor $(r_{\rm g}/R_{\rm L})^2$.

3.4.2. The magnetic field distribution

The normalized magnetic field distribution is prescribed by

– *the shape of the field line*, $z(x)$,
– *the magnetic flux distribution*, $\Phi(x) = \tilde{\Phi}(x)\sqrt{-g/(\rho^2\Delta)}$.

We apply different functions $z(x)$ and $\tilde{\Phi}(x)$ in order to investigate the influence of collimation, rotation and magnetic flux distribution on the jet acceleration. The function $z(x)$ we choose (i) weakly collimating and anchored close to the black hole, (ii) rapidly collimating and anchored close to the black hole, (iii) rapidly collimating and anchored at some distance from the black hole. One example for the shape of the flux surface is $z = 0.1(x-x_0)^{6/5}$, which describes a rather conical surface with only a slight collimation (solution S4, S4b, see Fig. 2). A possible choice for the magnetic flux distribution is $\tilde{\Phi}(x) = (x/x_{\star})^{-1/2}$, resulting in magnetic flux function $\Phi(x)$ decreasing with radius faster than a monopole where $\Phi(x) = 1$.

Clearly, the amount of magnetic energy available for acceleration at a certain position is a function of space $B_{\rm p}^2(r,\theta)$. That "opening" of the flux surfaces being related to the *two-dimensional* field distribution is not known in general. Depending on the intrinsic field generation mechanism the field strength decreases with radius. For a monopole type field distribution (for which $\Phi =$ const.) the field strength decreases with $\sim r^{-2}$ as for a dipole type distribution we have $\sim r^{-3}$. Our choice for the flux function Φ is between these cases.

Prescribing both the flux distribution and the shape of the flux surface does not over-determine the problem. The magnetic flux function Φ describes the opening of the magnetic flux tubes. With the *shape* of the flux surface chosen, the choice of the flux *function* just defines the position of the "other" flux surfaces. In a fully self-consistent approach, the field structure is determined by the solution of the Grad-Shafranov equation. Such solutions are not yet available.

3.4.3. The plasma temperature

The temperature distribution along the field line follows a polytropic gas law, $T = T_{\star}\,(n/n_{\star})^{\Gamma-1}$. In our approach the temperature at the injection radius $x_{\star}$ is determined by choosing the sound speed at this point, $c_{\rm s\star}$,

$$T_{\star} = \frac{\Gamma-1}{\Gamma} \left(\frac{c_{\rm s\star}^2}{\Gamma - 1 - c_{\rm s\star}^2}\right) \frac{m_{\rm p}c^2}{k_{\rm B}} \tag{9}$$

For typical parameters applied in our calculations, $c_{\rm s\star} = 0.05$, $\Gamma = 5/3$ this gives a gas temperature of the disk corona of about 1.5×10^{10}K at the jet injection radius. This temperature is in rough agreement with the disk temperature of the advection dominated accretion disk models at small radii (Narayan et al. 1998).

3.4.4. The iso-rotation parameter $\Omega_{\rm F}$

The iso-rotation parameter $\Omega_{\rm F}(\Psi)$ is determined from the position of the injection radius of the field line $x_{\star}$. This choice corresponds to the interpretation often applied for $\Omega_{\rm F}$ as the "angular rotation of the field lines". Here, we assume that the field lines are anchored in a Keplerian disk, $\Omega_{\rm F} \simeq \Omega_{\rm Disk} \simeq \Omega_{\rm K}(x_{\star})$. For a radial position not too close to the black hole, the angular velocity in the accretion disk follows its Newtonian value. Close to a black hole $\Omega_{\rm F}$ is limited due to the 'rotation of space' ω. A Keplerian disk would give $\Omega_{\rm F}(x_{\star}) \sim x_{\star}^{-3/2}$. An injection radius $x_{\star} = 8.3$ typical for our solutions gives $\Omega_{\rm F} = 0.04$ which is about $0.1\Omega_{\rm H}$.

4. Results and discussion

We now discuss our numerical solutions of the general relativistic magnetic wind equation for different field geometries and input parameters. With the prescribed poloidal field our solution is uniquely defined by the conditions along the jet foot point and the condition of regularity across the magnetosonic points. Due to the stationarity assumption and the prescription of the field distribution, the spatial range of the computation is in principle not limited in radius. This is essential if one considers the huge size of Galactic superluminal jets in terms of the size of the central object.

In general, we show that the acceleration of plasma from regions close to a black hole to the speed of $0.92\,c$ observed for

Table 1. Comparison of leading parameters for the wind solution. Magnetic flux distribution $\tilde{\Phi}/\tilde{\Phi}_\star$, shape of the poloidal field line $z(x)$, iso-rotation parameter $\Omega_{\rm F}$, sound speed at the injection radius $c_{\rm s\star}$, magnetization at the injection radius $\sigma_\star$, cylindrical Alfvén radius $x_{\rm A}$, cylindrical injection radius $x_\star$, total energy E, normalized to $m_{\rm p}c^2$ normalized total angular momentum $\tilde{L} = L/E$, asymptotic velocity $u_{\rm p\infty}$, and distance from the central object when this speed is reached $z(x(u_{\rm p\infty}))$. Other Parameters are: $u_{\rm p\star} = 0.0065$, $a = 0.8$, $\Gamma = 5/3$.

	prescribed		calculated								
	$\tilde{\Phi}/\tilde{\Phi}_\star$	$z(x)$	$\Omega_{\rm F}$	$c_{\rm s\star}$	$\sigma_\star$	$x_{\rm A}$	$x_\star$	E	$\tilde{L}$	$u_{\rm p\infty}$	$z(x(u_{\rm p\infty}))$
S3	~ 1	$0.1(x-x_0)^{6/5}$	0.035	0.05165	979.4	22.931	8.3	2.7887	20.03886	2.5	4×10^8
S3c	~ 1	$0.1(x-x_0)^{3/2}$	0.035	0.0525	3588	25.0	8.3	4.7383	23.54	$\simeq 5.5$	$\simeq 5 \times 10^6$
S4	$\sim x^{-1/2}$	$0.1(x-x_0)^{6/5}$	0.035	0.049	2380	22.931	8.3	2.7879	20.037	$\simeq 2.7$	$\simeq 10^5$
S4b	$\sim x^{-1/2}$	$0.1(x-x_0)^{6/5}$	0.014	0.03865	25850	60.53	15.3	3.5282	52.973	$\simeq 3.8$	$\simeq 2 \times 10^6$
S9	$\sim x^{-1/2}$	$0.1(x-x_0)^{3/2}$	0.035	0.05165	2777	22.92	8.3	2.7572	19.93	2.6	$\simeq 3000$

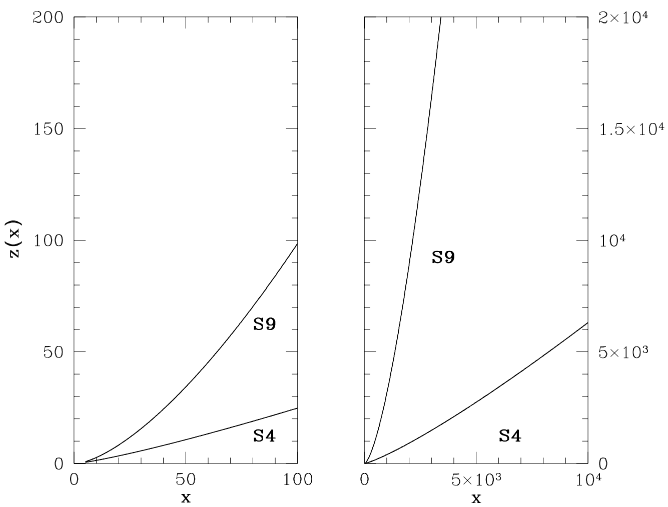

Fig. 2. Projected magnetic flux surface. Shape of the poloidal field line / flux surface as function $z(x)$ for the solutions S4 (and S4b, S3, S1) and S9 (and S3c).

Galactic superluminal motion is possible to achieve. Depending on the poloidal magnetic field distribution, the asymptotic speed of the jet is reached at a radius of about 100 gravitational radii.

For comparison the leading parameters for all 5 astrophysical examples are summarized in Tab. 1. Additionally, the example solution S1 shows the typical behavior of the solution branches in the case of super- or sub-critical parameters (Fig. C.1, Appendix C).

4.1. The wind solution – a collimating relativistic jet

Compared to the other examples, solution S3 (Fig. 3) is relatively weakly magnetized. The initial opening angle of the magnetic flux surface is large. The magnetic flux function $\tilde{\Phi}(x)$ is constant along the field line. Therefore, the magnetic acceleration is less efficient with magnetic flux being transformed into kinetic energy only slowly (compared to e.g. solution S4). The asymptotic poloidal velocity of $u_{\rm p} = 2.5$ is reached beyond a radius $x \simeq 10^8$ (corresponding to a distance from the black hole of $z(x) \simeq 4 \times 10^8$).

Figure 3 also shows the distribution of other physical parameters. The poloidal field strength $B_{\rm p}$ decreases with the opening of the magnetic flux surfaces. While the poloidal field distribution is prescribed in our approach, the toroidal magnetic field profile is a result of computation and therefore determined by the critical wind solution. At the injection point the toroidal field strength is about ten times smaller then the poloidal component. Outside the Alfvén radius the toroidal field becomes much larger than the poloidal component. For large radii the magnetic field helix is dominated by the toroidal component. We find that here the toroidal field component follows a power law distribution $d(\log B_\phi) \simeq d(\log x)$. Therefore, in the asymptotic part the poloidal electric current is almost constant $I \sim x B_\phi \sim {\rm const.}$ In relativistic MHD electric fields cannot be neglected. The electric field orientation is perpendicular to the magnetic flux surfaces and the field strength is $E_\perp = (R/R_L) B_P$. Therefore, the electric field is dominating the poloidal magnetic field outside the light cylinder.

The density and temperature distributions (Fig. 3) are interrelated by the polytropic gas law. At the injection point the gas temperature $T \simeq 10^{10}$K and density $\rho \simeq 0.1\,{\rm cm}^{-3}$ are comparable with the conditions in the inner disk (see Sect.3.4.3). Density and temperature decrease rapidly along the field line following a polytropic expansion. For $x \gtrsim$30 the proper mass density follows a power law $\rho \simeq 4 \times 10^{-5} x^{-1.8}$. At a radius $x \simeq 1000$ the gas temperature is about 10^6K. Therefore we can estimate the size of the X-ray emitting region of about several $1000\, r_{\rm g}$ in diameter. For the example of GRS 1915+105 this corresponds to 3.5×10^{-9} arcsec. It would be interesting to calculate the X-ray spectra of such an relativistically expanding high temperature gas distribution.

Solution S3c has the same distribution of the magnetic flux function Φ as solution S3. The magnetic flux surfaces, however, are collimating more rapidly. The derived critical wind solution has a large magnetization. The Alfvén radius comes closer to the light cylinder, although $\Omega_{\rm F}$ is the same in both solutions

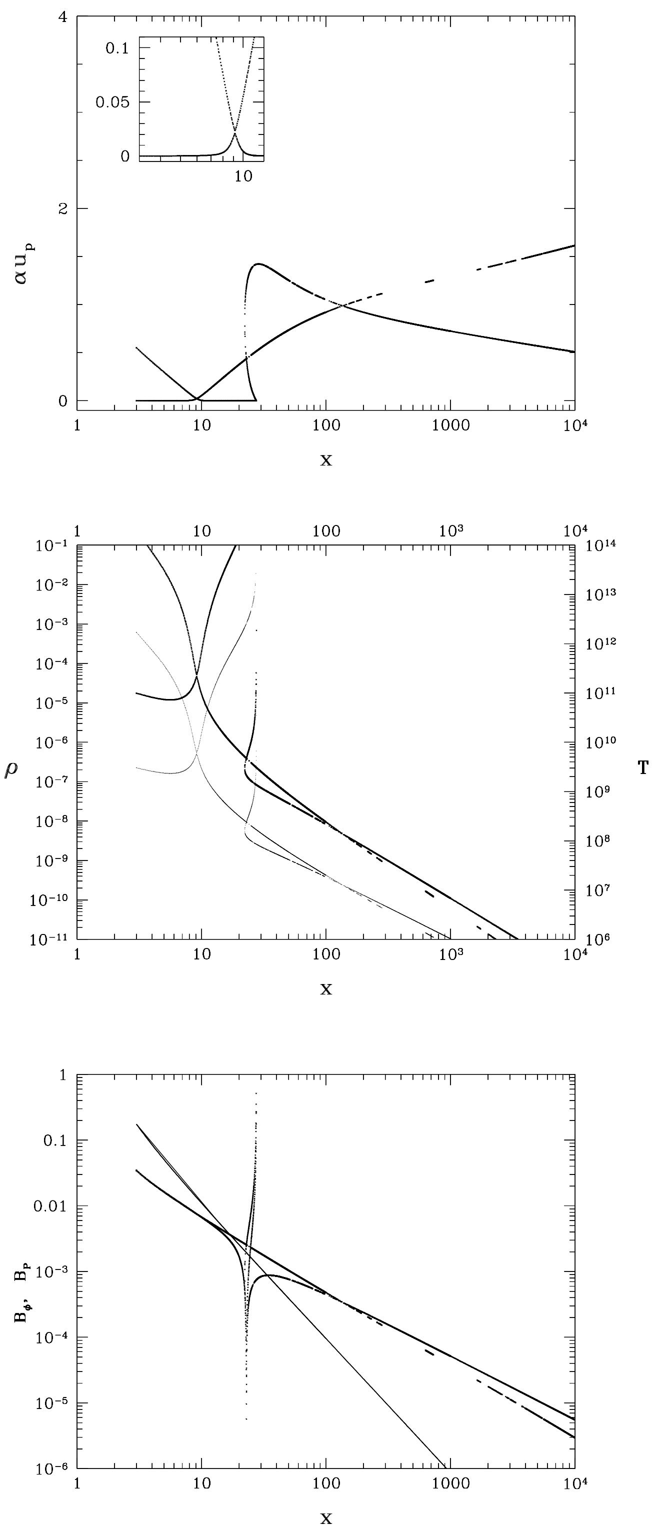

Fig. 3. Solution S3. Properties of the critical wind flow along a given flux surface (for the flow parameters see Tab. 1). Poloidal velocity $\alpha u_{\rm p}$ (in c), proper mass density ρ (in $\rm cm^{-3}$), temperature T (in K), poloidal and toroidal field strength, $B_{\rm p}, B_\phi$ (normalized to the magnetic flux at the injection radius). The asymptotic jet velocity of $u_{\rm p} = 2.5$ is reached after about $x = 10^8$. The critical (magnetosonic) points are located at the intersections of the two solution branches.

S3 and S3c. The terminal speed and the total energy density $E(\Psi)$ of the S3c solution is much larger. Because of the large magnetization type S3c jet solutions correspond to jets with a low mass flow rate.

Solution S9 relies on the same magnetic flux surface as S3c. The jet reaches its asymptotic velocity of $u_{\rm p} = 2.6$ already at $x = 100$. In this rapidly collimating field structure this position corresponds to a distance from the central black hole of about $z = 3000$. As a difference to S3c the magnetic flux function decreases with radius implying that the magnetic energy is slowly converted into kinetic energy and the terminal speed is correspondingly lower. This is interesting because it proves that not only the magnetization determines the asymptotic speed, but also the distribution of the magnetic flux along the field line.

Solution S4 has the same magnetic flux distribution as S9, however, the field line is only weakly collimating. The asymptotic jet speed and the magnetization parameter is about the same. Only, the initial acceleration is weaker because the magneto-centrifugal mechanism works less efficient in the field with a smaller opening angle.

Solution S4b has essentially the same field distribution as S4, but the injection radius is chosen larger. Therefore, the iso-rotation parameter $\Omega_{\rm F}$ is decreased by a factor of $(8.3/15.3)^{3/2}$ following a quasi Keplerian angular velocity of the field line's foot points. As a result, the critical wind solution could be obtained only for a very high plasma magnetization and the terminal jet velocity is large. Such a solution is feasible if the mass flow rate in the jet decreases with radius faster than the field strength (or flux distribution). This proves that highly relativistic jets can be expected even if the jet is not emerging from a region close to the black hole. The question remaining is whether the required high field strengths can be found at these positions.

We summarize the results of this section. The asymptotic speed is determined by the plasma magnetization and the distribution of the magnetic flux along the field line. The shape of the magnetic flux surface determines the velocity *profile* along the field, thus, the position where the asymptotic velocity is reached. Highly relativistic outflows can be obtained even if the jet foot point is *not* very close to the black hole. However, in this case a high plasma magnetization is necessary. seems to be in contradiction to the accretion disk theory (see below).

4.2. The question of magnetization

The magnetic acceleration of jets and winds can be understood either as a consequence of conversion of Poynting flux (magnetic energy) to kinetic energy or due to Lorentz forces along the poloidal field line. Thus, the higher the plasma magnetization the more energy can be transformed into kinetic energy of the wind. It has been shown theoretically that the relation between magnetization and asymptotic velocity is that of a power law, $u_{\rm P\infty} \sim \sigma^{1/3}$, for conical outflows (Michel 1969) and for collimating flows (Fendt & Camenzind 1996), if the flux distribution is the same, respectively. However, both papers do not consider gravity (and not general relativistic effects). The new solutions presented in this paper are in general agreement with

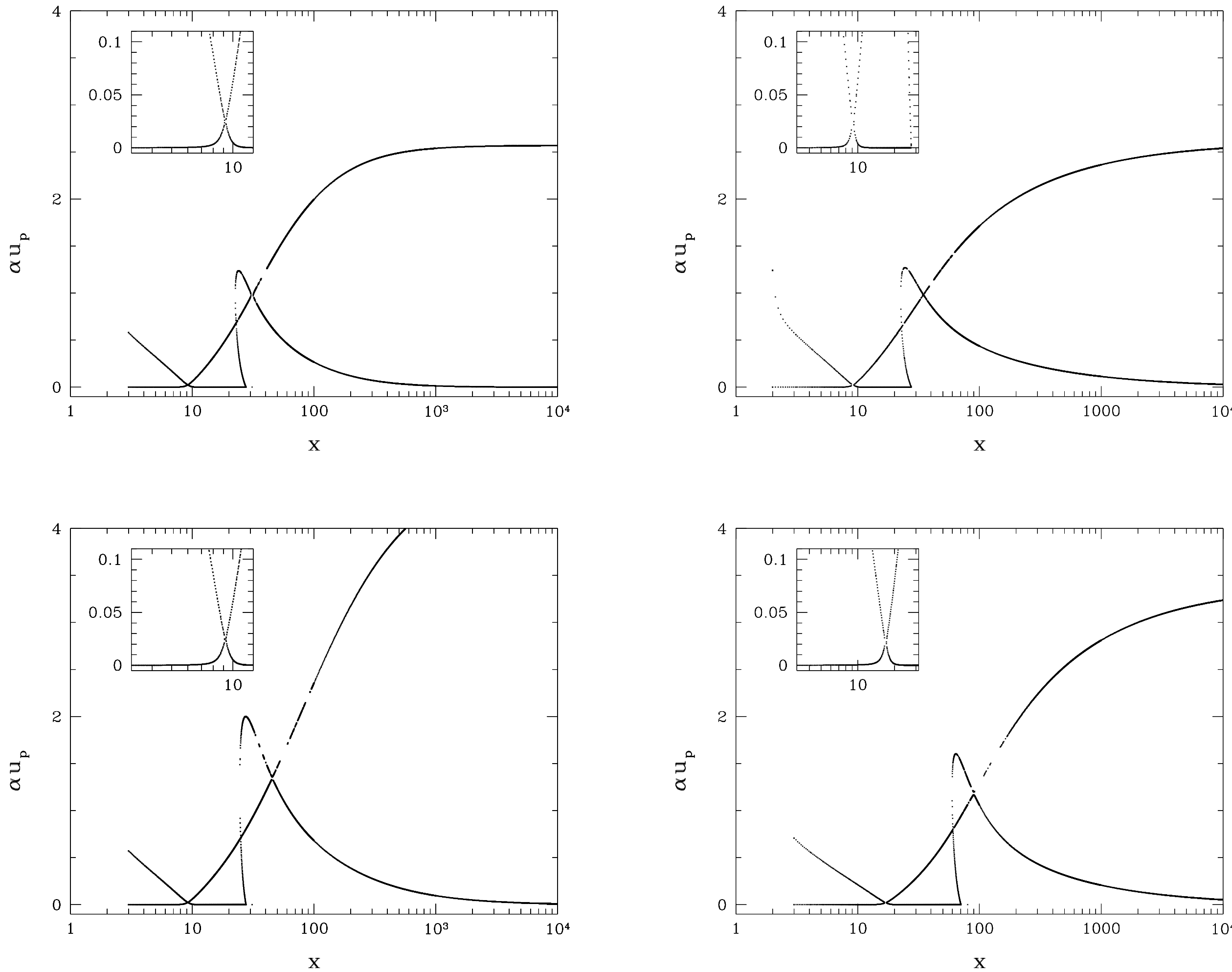

Fig. 4. Solutions S9 (*upper left*), S3c (*lower left*), S4 (*upper right*), S4b (*lower right*). Poloidal velocity $\alpha u_{\rm p}$ along the field line in units of the speed of light. For the solution parameters see Tab. 1.

those results. The power law distribution is, however, not exactly obtained, since other parameters vary between the different solutions.

The wind magnetization is determined by the disk properties at the jet injection points along the disk surface. For a standard thin disk model that the ratio of the mass flow rate in the jet to the disk accretion rate is about 1% (Ferreira 1997). The observational data for various jet-disk systems are consistent with this theoretical value. The accretion disk magnetic flux can be estimated assuming equipartition between magnetic field pressure (energy) and gas pressure (thermal energy) in the disk (see Sect. 3.4.1). From Eq. (7) we find an equipartition field strength of about $B_{\rm eq} \simeq 5 \times 10^8$G, if $\alpha_{\rm vis} \simeq 0.1$ and $R_{\star} = 10 r_{\rm g}$. Equation (8) then defines an upper limit for the plasma magnetization at the injection radius, $\sigma_{\star} = 5 \times 10^4$, for $\dot{M}_{\rm jet} \simeq 0.1 \dot{M}_{\rm acc}$. Such a value is in general agreement with our solutions (Tab. 1). The maximum equipartition field strength estimated with the above given formulae can be much larger for Galactic black hole jet sources as for AGN (see Eq. 7). For a low black hole mass (with a smaller horizon) the disk comes closer to the singularity and therefore becomes hotter.

Finally, we come back to the examples S4 and S4b. As already mentioned, these solutions demonstrate that the jet origin must not be necessarily close to the black hole. One may think that a strong magnetization at larger disk radii would do the job. On the other hand, the equipartition field strength in the disk decreases with radius implying that the highest magnetization and, thus, jet velocities must be expected from the inner part of the disk. Only, if the mass transfer rate from the disk into the jet decreases more rapidly with radius than the field strength, the *magnetization* increases.

4.3. The question of collimation

The huge size observed for the knots of the Galactic superluminal sources leaves the possibility that the jet is basically *un-collimated*.

Our numerical solutions have shown that the asymptotic speed of the jet does not depend very much on the degree of collimation in the flow. That speed is reached within a distance of about $10^8 r_{\rm g}$. However, the observed upper limit for the knot size is still a factor 10 larger. Therefore, from our solutions, the observed knots are consistent with both a collimated and an un-collimated jet flow. In particular, solution S9 which is more collimated, has the same asymptotic speed as solution S4.

In the case of extragalactic jets a high degree of collimation is indicated. The "lighthouse model" by Camenzind & Krockenberger (1992) gives opening angles of only $0\overset{\circ}{.}1$ for the quasar 2C273 or $0\overset{\circ}{.}05$ for typical BL Lac objects. The question arises whether there could be an intrinsic difference between the jets of AGN and Galactic high energy sources. Why should Galactic superluminal jets be un-collimated? A difference in the jet magnetization seems to be unlikely since the jet velocities are comparable. We hypothesize that if the jets of these sources are systematically different, this should rather be caused by the conditions in the jet environment. If the jets are collimated by external pressure, a different external/internal pressure ratio will affect the degree of jet collimation. Extragalactic jets are believed to be confined by the interstellar matter in the galaxy bulge. It is likely that Galactic superluminal sources provide an example where the jet pressure exceeds the pressure of the ambient medium. While AGN jets bore a funnel through the galactic bulge, Galactic superluminal jets freely expand into the empty space. Such a picture seems to be supported by the fact that the Galactic superluminal jet knots move with constant velocity over a long distance.

5. Summary

We have investigated magnetically driven superluminal jets originating from a region close to a rotating black hole. The stationary, general relativistic, magnetohydrodynamic wind equation along collimating magnetic flux surfaces was solved numerically. The wind solutions were normalized to parameters typical for Galactic superluminal sources.

The assumption of stationarity allows us to calculate the jet velocity on a *global* scale over a huge radial range in terms of radius of the central source. The wind is launched close to the rotating black hole at several gravitational radii. The calculation was performed up to a radius of 10 000 gravitational radii, but is in general not limited in radius. Different magnetic field geometries were investigated. The model allows for a choice of the *shape* of the magnetic flux surface *and* the *flux distribution* of that field.

The physical wind solution is defined by the regularity condition at the magnetosonic points. As the poloidal field is prescribed, the choice of the following input parameters determines the wind solution completely, (i) the injection radius of the matter into the jet, (ii) the injection velocity and (iii) the plasma magnetization (the ratio of magnetic flux to mass flux). The results of our numerical computation are the following.

- In general, the observed speed for Galactic superluminal sources of more than 0.9 c can be achieved.
- For a fixed magnetic field distribution the asymptotic jet velocity depends mainly on the plasma magnetization, in agreement with earlier papers (Michel 1969, Fendt & Camenzind 1996). The higher the plasma magnetization, the higher the final speed. The velocity distribution along the magnetic field shows a saturating profile depending on the distribution of the magnetic flux.
- The magnetic flux distribution along the field line also influences the plasma acceleration. Since the real field distribution is not known, we have considered two cases which show the typical behavior and which are probably close to the reality. We find that the jet velocity in a (spatially) faster decaying field is lower (for the same magnetization).
- For jet solutions *not* emerging from a region close to the black hole, a highly relativistic velocity can be obtained if the flow magnetization is sufficiently large. However, one we hypothesize that the field strength required for such a magnetization can be generated only close to the black hole.
- Investigation of two different jet opening angles has shown that both field distributions allow for a relativistic velocity. The asymptotic jet velocity is reached considerably earlier in the case of the faster collimating flux surface. For a opening angle of the flux surfaces of about 15°(45°) the asymptotic speed is reached at a distance from the injection point of $3000 r_{\rm g}$ ($10^5 r_{\rm g}$). This distance is below the observational resolution by several orders of magnitude. Therefore, the question of the degree of collimation for the superluminal jets of GRS 1915+105 and GRO 1655-40 could not be answered by our approach.
- Motivated by the huge size of the observed knots in the Galactic superluminal jets, we point out the possibility that the jet collimation process in these sources may be intrinsically different in comparison to the AGN. For example, the upper limit for the knot diameter in GRS 1915+105 is about 10^9 Schwarzschild radii, which is distinct from typical estimates for AGN jets with diameters of about 100 - 1000 Schwarzschild radii.
- The gas temperature at the injection point is about 10^{10}K which is one order larger then the disk temperature at this point. With the polytropic expansion the temperature decreases rapidly to about 10^6K at a distance of 5000 Schwarzschild radii from the source. Both the temperature and the mass density follow a power law distribution with the radius.
- The calculations show that the jet magnetic field is dominated by the toroidal component. Similarly, the velocity field is dominated by the poloidal component.

In summary, our numerical calculations have shown that the highly relativistic speed observed for galactic superluminal sources may be achieved by magnetic acceleration. For a given magnetic flux surface we obtain the complete set of physical parameters for the jet flow. The calculated temperature, density and velocity profile along the jet would provide a promising set of input parameters for a computation of the spectral energy distribution.

Acknowledgements. C.F. acknowledges helpful discussions with Mikael Jensen at Lund Observatory.

Appendix A: Parameters of Kerr metric

For the reason of completeness, here we list the parameters applied in the equations of Kerr geometry. In Boyer-Lindquist coordinates with the parameters

$$\begin{aligned} \rho^2 &\equiv r^2 + a^2 \cos^2\theta, & \Delta &\equiv r^2 + a^2 - 2M\,r, \\ \Sigma^2 &\equiv (r^2+a^2)^2 - a^2\Delta\sin^2\theta, & \tilde\omega &\equiv (\Sigma/\rho)\,\sin\theta, \\ \omega &\equiv 2\,a\,M\,r/c\,\Sigma^2, & \alpha &\equiv \rho\sqrt{\Delta}/\Sigma, \end{aligned}$$

the components of the metric tensor are defined as

$$\begin{aligned} g_{00} &= \sigma_{\rm m}(2r/\rho(r,\theta)^2 - 1) \\ g_{03} &= -\sigma_{\rm m} 2ra\sin(\theta)^2/\rho(r,\theta)^2 \\ g_{11} &= \sigma_{\rm m}\rho(r,\theta)^2/\Delta(r,\theta) \\ g_{22} &= \sigma_{\rm m}\rho(r,\theta)^2 \\ g_{33} &= \sigma_{\rm m}\Sigma(r,\theta)^2\sin(\theta)^2/\rho(r,\theta)^2 \\ g &\equiv {\rm Det(g_{\mu\nu})} = -g_{11}g_{22}(g_{30}^2 - g_{00}g_{33}) \end{aligned}$$

In our paper we have chosen a negative sign of the metric, $\sigma_{\rm m} = -1$.

Appendix B: Wind polynomial

Here we provide the polynomial coefficients of the general relativistic magnetohydrodynamic wind equation Eq. (4). For a derivation, see Camenzind (1986), Takahashi et al. (1990), or Jensen (1997). The specific angular momentum, properly normalized, is

$$\tilde L = -(g_{03} + \Omega_{\rm F}\,g_{33})/(g_{00} + \Omega_{\rm F}\,g_{03}) \qquad \text{(B1)}$$

For convenience we define the following parameters,

$$\begin{aligned} C_1 &= \frac{c_{\rm s\star}^2}{\Gamma - 1 - c_{\rm s\star}^2}\left(u_{\rm p\star}\sqrt{\frac{g_\star}{g}}\frac{\Phi}{\Phi_\star}\right)^{\Gamma-1}, \quad C_2 = \sqrt{-g}\frac{\Phi_\star}{\Phi\sigma_\star} \\ D_1 &= g_{00} + 2\Omega_{\rm F}g_{03} + \Omega_{\rm F}^2 g_{33}, \quad D_2 = (1-\Omega_{\rm F}\tilde L)^2 \\ D_3 &= -(g_{33} + 2\tilde L g_{03} + \tilde L^2 g_{00})/(g_{03}^2 - g_{00}g_{33}) \end{aligned}$$

With the corresponding values at the injection radius $x_\star$ the total specific energy density of the flow E is defined as

$$E^2 = \frac{-\sigma_{\rm m}\mu_\star^2(u_{\rm p\star}^2+1)(D_{1\star}+\sigma_{\rm m}M_\star^2)^2}{(D_{1\star}+2\sigma_{\rm m}M_\star^2)D_{2\star} + D_{3\star}M_\star^4} \qquad \text{(B2)}$$

The polynomial coefficients of the wind equation (4) are

$$\begin{aligned} \tilde a_{1,2n+2m} &= C_2^2 \\ \tilde a_{2,2n+m} &= 2\sigma_{\rm m}C_2D_1 \\ \tilde a_{3,2n} &= D_1^2 + C_2^2 + \sigma_{\rm m}E^2C_2^2D_3 \\ \tilde a_{4,2n-m} &= 2\sigma_{\rm m}C_2D_1 + 2E^2C_2D_2 \\ \tilde a_{5,2n-2m} &= D_1^2 + \sigma_{\rm m}E^2D_1D_2 \\ \tilde a_{6,n+3m} &= 4C_1C_2^2 \\ \tilde a_{7,n+2m} &= 6\sigma_{\rm m}C_1C_2D_1 \\ \tilde a_{8,n+m} &= 2C_1D_1^2 + 4C_1C_2^2 + \sigma_{\rm m}2E^2C_1C_2^2D_3 \\ \tilde a_{9,n} &= \sigma_{\rm m}6C_1C_2D_1 + 2E^2C_1C_2D_2 \\ \tilde a_{10,n-m} &= 2C_1D_1^2 \\ \tilde a_{11,4m} &= 6C_1^2C_2^2 \\ \tilde a_{12,3m} &= 6\sigma_{\rm m}C_1^2C_2D_1 \\ \tilde a_{13,2m} &= C_1^2D_1^2 + 6C_1^2C_2^2 + \sigma_{\rm m}E^2C_1^2C_2^2D_3 \\ \tilde a_{14,m} &= 6\sigma_{\rm m}C_1^2C_2D_1 \\ \tilde a_{15,0} &= C_1^2D_1^2 \\ \tilde a_{16,5m-n} &= 4C_1^3C_2^2 \\ \tilde a_{17,4m-n} &= 2\sigma_{\rm m}C_1^3C_2D_1 \\ \tilde a_{18,3m-n} &= 4C_1^3C_2^2 \\ \tilde a_{19,2m-n} &= 2\sigma_{\rm m}C_1^3C_2D_1 \\ \tilde a_{20,6m-2n} &= C_1^4C_2^2 \\ \tilde a_{21,4m-2n} &= C_1^4C_2^2 \end{aligned}$$

All coefficients with the same second index have to be summed up, $A_i = \sum_j \tilde a_{j,i}$. The polytropic indices $n=5$, $m=6$ give a polynomial of 16th order.

Appendix C: Example wind solution in Kerr metric

Here we show an example solution of the wind equation (4). The parameters are chosen such that a variation of $\sigma_\star$ and $c_{\rm s\star}$ clearly demonstrates the criticality of the wind solution. They do not necessarily match astrophysical constraints. However, the asymptotic poloidal velocity is comparable to the speed of the Galactic superluminal sources. The solution (solution S1) considers a highly magnetized plasma flow with $\sigma_\star \simeq 5\,10^4$. The flux geometry is that of a slightly collimating cone with an opening angle decreasing with distance from the source.

Figure C1 shows the solution branches with a positive $u_{\rm p}^2$. An overlay of solutions for three parameter sets is displayed in order to show the typical behavior of wind solution. There is only one unique solution, the critical solution, with one branch continuing from small to large radii without any gaps in $u_{\rm p}$ or x. The magnetosonic points are located at the intersections of the solution branches of the critical solution. The *critical* wind solution is regular at all three magnetosonic points. It is defined by a *unique* set of the parameters E, L and σ (for $\Omega_{\rm F}$ prescribed). In the critical solution the slow magnetosonic point is passed close to the foot point of the jet. The Alfvén point is located at $x = 31$ and the fast magnetosonic point not far beyond.

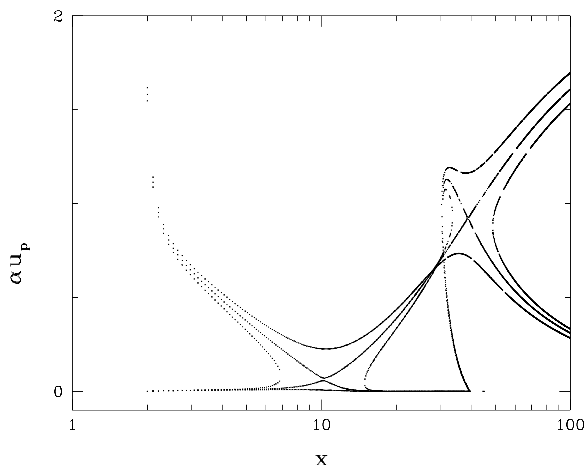

Fig. C1. Example solution S1. Overlay of solutions $u_{\rm p}(x)$ for three different parameter sets. $\sigma_\star = 49830$, $c_{\rm s\star} = 0.4585$ gives the critical solution which is regular across the magnetosonic points. The critical *wind* solution is the continuous branch starting with low velocity and accelerating to high speed. The magnetization $\sigma_\star$ is the critical parameter for the FM point, whereas $c_{\rm s\star}$ is the critical parameter for the SM point. Sub- or super-critical solutions are obtained by variation of the parameters $\sigma_\star$, $c_{\rm s\star}$. The choice of $\sigma_\star = 51830$, $c_{\rm s\star} = 0.4485$ results in gaps in $x(u_{\rm p})$, the choice of $\sigma_\star = 48830$, $c_{\rm s\star} = 0.4685$ in gaps in $u_{\rm p}(x)$. The other parameters are $x_{\rm A} = 31.2$, $u_{\rm p\star} = 0.01$, $x_\star = 3.0$, $\Omega_{\rm F} = 0.1\,\Omega_{\rm H} = 0.025$, $a = 0.8$.

The asymptotic speed of the flow is $u_{\rm p} = 2.28$, equivalent to $v_{\rm p} \simeq= 0.9\,c$ (not shown in the Figure).

Sub- or super-critical wind parameters lead to solution branches which are not defined for all radii or all velocities. Even for a slight variation of these parameters the solution will be not continuous anymore, implying “jumps” or “shocks” across the gaps in the solution branches. At these locations the stationary character of the solution most probably breaks down. Such solution branches are inconsistent with the assumptions and are therefore referred to as *unphysical*.

References

Belloni T., Mendez M., King A.R., van der Klis M., van Paradijs J., 1997, ApJ, 479, L145
Beskin V.S., Pariev, V.I., 1993, Physics Uspekhi, 36, 529
Beskin V.S., 1997, Physics Uspekhi, 40, 659
Blandford R.D., Znajek R.L., 1977, MNRAS, 179, 433
Blandford R.D., Payne D.G., 1982, MNRAS, 199, 883
Blandford R.D., 1990, in: R.D. Blandford, H. Netzer, L. Woltjer, Active Galactic Nuclei, T.J-L. Courvoisier, M. Mayor (eds), Lecture Notes, Saas-Fee Advanced Course 20, Springer, Heidelberg, p.242
Brandenburg A., 1996, ApJ, 465, L115
Camenzind M., 1986, A&A, 162, 32
Camenzind M., 1987, A&A, 184, 341
Camenzind M., Krockenberger, M., 1992, A&A, 225, 59
Eikenberry S.S., Matthews K., Morgan E.H., Remillard R.A., Nelson R.W., 1998, ApJ, L61
Englmaier P., 1993, Diploma Thesis, University of Heidelberg
Fender R., Garrington S.T., McKay D.J. et al. 1999, MN 304, 865
Fender R., 2000: *Astrophysics and Cosmology: A collection of critical thoughts*, Lecture Notes in Physics, Springer (in press; astro-ph/9907050)
Fendt C., Camenzind M., 1996, A&A, 313, 591
Fendt C., 1997, A&A, 319, 1025
Ferreira, J, 1997, A&A, 319, 340
Gliozzi M., Bodo G., Ghisellini G., Scaltriti F., Trussoni E., 1998, A&A, 337, L39
Greiner J., Morgan E.H., Remillard R.A., 1996, ApJ, 473, L107
Greiner J., Morgan E.H., Remillard R.A., 1998, New Astr. Rev. 42, p. 597
Greiner J., 2000, in Cosmic Explosions, Proc. 10th Ann. Maryland Astrophys. Conf., eds. S. Holt, W.W. Zhang, AIP (in press; astro-ph/9912326)
Hjellming R.M., Rupen M.P., 1995, Nature, 375, 464
Hardee P.E., Rosen A., Hughes P.A., Duncan G.C., 1998, ApJ, 500, 599
Jensen M., 1997, General relativistic MHD winds from supermassive black holes, Master Thesis, Lund Observatory
Khanna R., Camenzind M., 1996a, 307, 665
Khanna R., Camenzind M., 1996b, 313, 1028
King A.R., Kolb U., 1999, MNRAS, 305, 654
Koide S., Shibata K., Kudoh T., 1998, ApJ, 495, L63
Koide S., Meier D.L., Shibata K., Kudoh T., 2000, ApJ, 536, 668
Kuulkers E., Wijnands R., Belloni T., Mendez M., van der Klis M., van Paradijs J., 1998, ApJ 494, 753
Michel F.C., 1969, ApJ, 158, 727
Mirabel I.F., Rodriguez, L.F., 1994, Nature, 371, L46
Mirabel I.F., Rodriguez, L.F., 1995, Superluminal motion in our Galaxy, in: Proceedings of the 17th Texas Symposium on Relativistic Astrophysics, in press
Mirabel I.F., Dhawan V., Chaty S., et al. 1998, A&A 330, L9
Mioduszewski A.J., Hughes P.H., Duncan G.C., 1997, ApJ 476, 649
Morgan E.H., Remillard R.A., Greiner J., 1997, ApJ 482, 993
Narayan R., Mahadevan R., Quataert E., 1998, Advection-dominated accretion around black holes, in: Theory of Black Hole Accretion Disks, s M.A. Abramowicz, G. Bjornsson, J.E. Pringle (eds), Cambridge University Press, p.148
Nishikawa K.-I., Koide S., Dakai J.-I., Christodoulou D.M., Sol H., Mutel R.L., 1997, ApJ, 483, L45
Okamoto I., 1992, MNRAS, 254, 192
Orosz J.A., Bailyn C.,D., 1997, ApJ, 477, 876
Rodriguez, L.F., Mirabel I.F., 1999, ApJ, 511, 398
Scaltriti F., Bodo G., Ghisellini G., Gliozzi M., Trussoni E., 1997, A&A, 325, L29
Thorne, K.S., Price, R.H., Macdonald, D., 1986, Black Holes: The membrane paradigm, Yale University Press, New Haven and London (TPM)
Tingay S.J., Jauncey D.L., Preston R.A., 1995, Nature, 374, 141
Takahashi M., Nitta S., Tatematsu Y., Tomimatsu A., 1990, ApJ, 363, 206
Ueda Y., Inoue H., Tanaka Y., Ebisawa K., Nagase F., Kotani T., Gehrels N., 1998, ApJ 492, 782
Zensus J.A., Cohen M.H., Unwin S.C., 1995, ApJ, 443, 35
Zhang N.S., Cui W., Chen W., 1997, ApJ 482, L155
Znajek R.L., 1977, MNRAS, 179, 457